Supporting Information For

Eutectic electrolyte based on N-Methylacetamide for highly reversible zinc-iodine battery

Yongqiang Yang,[a] Shuquan Liang, [a] Bingan Lu,[b] and Jiang Zhou,[a,c] *

[a] *School of Materials Science and Engineering, Key Laboratory of Electronic Packaging and Advanced Functional Materials of Hunan Province, Central South University, Changsha 410083, China, E-mail: zhou_jiang@csu.edu.cn.*

[b] *School of Physics and Electronics, Hunan University, Changsha 410083, China.*

[c] *College of Chemistry and Chemical Engineering, Jishou University, Jishou 416000, China.*

Experimental section

Preparation of N-Methylacetamide based eutectic electrolyte

All the reagents mentioned were from Aladdin. The preparation of eutectic electrolyte is achieved by *in situ* heating at 70℃ until becoming clear in sealed containers. Firstly, series precursor mixtures were prepared by adding $Zn(CF_3SO_3)_2$ and N-Methylacetamide with different molar ratio of 1:2, 1:4, 1:6 and 1:8 (denoted as 12, 14, 16, 18) to compare the effects of different Zn^{2+} concentration. Then, 0.5M, 1.0M or 2.0M KI was added based on the volume of precursor solutions (denoted as 14-05, 14-10, 14-20 taking 14 solution as an example) as the only source of iodine in this system. Finally, 20%, 40%, 60% or 80% volume fractions of deionized water were added to improve the viscosity and conductivity (denoted as 14-05-20, 14-05-40, 14-05-60, 14-05-80 taking 14-05 solution as an example), in which the influence of H_2O content was investigated.

Preparation of electrode and fabrication of zinc-iodine battery

Metal zinc foil without any modification was used as anode. The hydrophilic carbon fiber cloth (0.5×0.5 cm^2, W0S1009, CeTech Co., Ltd) was used as current collector, which was sonicated in deionized water, alcohol, acetone in sequence to remove impurities and then heated in nitric acid at 80°C for 3h to enhance the hydrophilicity. The cathode was prepared by mixing activated carbon (YP-50F, Kuraray Co., Ltd) and Polyvinylidene fluoride with a weight ratio of 9:1 in N-Methyl pyrrolidone solvent, which then was coated on caron fiber cloth and kept at 80℃ overnight in a vacuum oven. The calculated mass loading of activated carbon in the final cathode is about 2 mg (or 8 mg cm^{-2}). The coin cells (CR2016) were assembled by sandwiching glass microfiber filters (Whatman) soaked with electrolytes between the electrodes an open atmosphere. Particularly, the volume of the electrolyte used in each cell was fixed at 100 μL. Meanwhile, aqueous electrolyte (2M $Zn(CF_3SO_3)_2$ + 0.5M KI) was also performed for comparison.

Material characterizations

The Raman and UV-vis adsorption spectra of electrolytes were measured by RENISHAW *in suit* Raman microscope and Persee TU-1901 double beam UV-vis spectrophotometer at room temperature. The crystallographic phases of electrodes were determined by the Rigaku D/max 2500 X-ray powder diffractometer with Cu Kα-radiation (λ = 0.15405 nm). The morphologies with corresponding energy

dispersive spectrometer (EDS) mappings were collected by the FEI Nova NanoSEM-230M scanning electron microscopy (SEM), and the Titan G2 60-300 transmission electron microscopy (TEM) was performed to scan High-resolution TEM (HRTEM) images, selected area electron diffraction (SAED) patterns and EDS mappings. The X-ray photoelectron spectroscopy (XPS) used to reflect the evolution of valance in elements was recorded by ESCALAB 250 Xi X-ray photoelectron spectrometer.

Electrochemical measurements

Cyclic voltammetry (CV), linear sweep voltammetry (LSV), chronoamperometry (CA) and linear polarization curves were measured using the CHI660E. Electrochemical impedance spectroscopy (EIS) from 100 kHz to 10 mHz were conducted using the MULTI AUTOLAB M204. Galvanostatic charge-discharge (GCD) measurements were performed utilizing the LAND CT2001A.

Electrochemical performance evaluation standard

The addition of a fixed amount of electrolyte makes it possible to calculate the maximum capacity (Q_{max}, mA h) of its component KI in the case of single electron transfer. The formula is as follow:

$$Q_{max} = n\,V\,c\,\frac{N_A\,Q_e}{3.6} \approx 2.68 \times 10^4\,n\,V\,c$$

When n represents the electron transfer number of the reactant. V and c are respectively the dosage of electrolyte (L) and the molar concentration of the reactants (mol L^{-1}). N_A is the Avogadro constant as well as Q_e is the elementary charge. It is calculated that the Q_{max} of 14-05-20 solution which mainly used for the electrochemical measurement is 1.12 mA h. Taking into account the close influence of the cathodic area on the reversible capacity, the electrochemical performance of this zinc-iodine battery is presented in terms of the areal capacity.

Molecular dynamics simulations

Molecular dynamics (MD) simulation were carried out to investigate the structural evolutions of the 2M $Zn(CF_3SO_3)_2$ + 0.5M KI aqueous solution (including $Zn(CF_3SO_3)_2$, KI, H_2O) and the 14-05-20 eutectic solution (including $Zn(CF_3SO_3)_2$, KI, C_3H_7NO, H_2O), respectively.

The calculation was conducted on the structures of additives with an integration time-step of 2 fs, and the periodic boundary conditions were applied in the x- and y-dimensions. The box size of these

bulk systems was limited in $4.4 \times 4.4 \times 4.4$ nm^3. First, the conjugate gradient algorithm and energy minimization were performed to obtain the stable structures, which were further optimized through the condensed-phased optimized molecular potential for the atomistic simulation studies force field in Materials Studio with forcite module. Each system then was equilibrated under the constant-pressure–constant-temperature (NPT) ensemble at a constant temperature of 300 K to achieve an equilibrium state with zero pressure for 100 ns. Moreover, a potential cutoff radius of 2.25 nm was applied in the calculation of the non-bonded interaction, and the electrostatic was described by the particle-particle particle-mesh (PPPM). The Andersen feedback thermostat and Berendsen barostat algorithm were applied with temperature and pressure conversion. Finally, the properties of solvated structures were received in the last 5 ns.

The radial distribution functions (RDFs) which reflected the probability of the distances between the atoms were calculated using the VMD analysis tool.

The Gibbs free-energy calculation of iodine reductions was also based on the frequency of each complex after geometric optimization. The adsorption energy (*E(ad)*) of I_2 was defined according to the following equation:

$$E(ad) = E(total) - E(surface) - E(I_2)$$

where *E(total)*, *E(surface)* and $E(I_2)$ represented to the energy of the surface with adsorbed I_2, clean surface and I_2 molecule, respectively. The more negative the value of *E(ad)* mean the stronger adsorption effect. Based on this, the free-energy of iodine reductions were further obtained according to the following equation:

$$\Delta G = E(gs) + E(zp) - T\Delta S$$

where *E(gs)*, *E(zp)* and $T\Delta S$ were the ground-state energy, zero-point energy and entropy term, respectively, with the latter two taking vibration frequencies from the density functional theory (DFT) calculation. On the other hand, the free-energy (ΔG) of different intermediates were also defined as:

$$\Delta G = E(i) - E(reactant)$$

where the *E(i)* was the energy of intermediates and *E(reactant)* was the total energy of reactants.

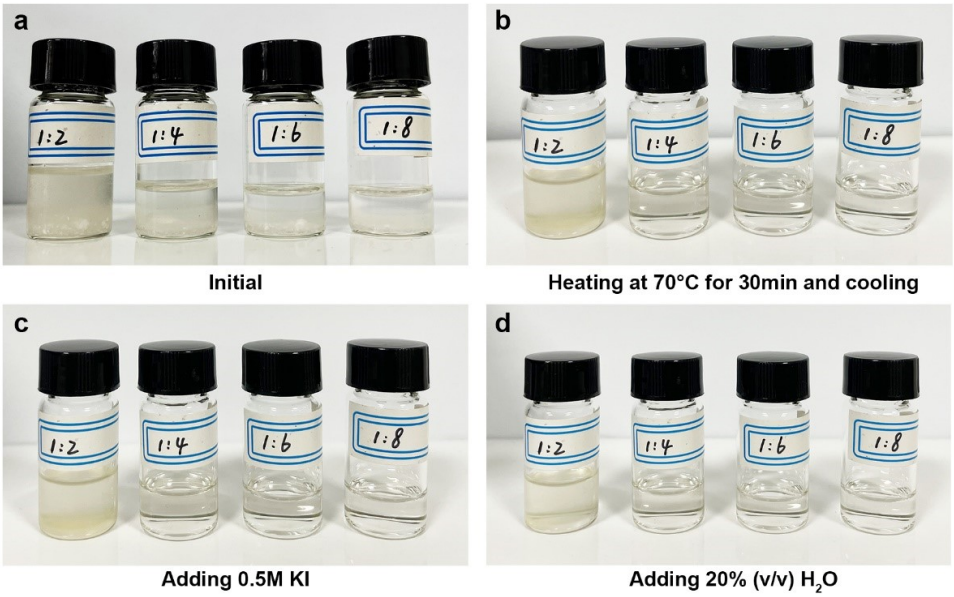

Figure S1. Optical images of (a) mixtures of $Zn(CF_3SO_3)_2$/N-ACE with different molar ratios (1:2-1:8) and (b) eutectic solutions after heating and cooling (denoted as 12, 14, 16, 18). (c) Eutectic solutions after adding 0.5M KI (denoted as 12-05, 14-05, 16-05, 18-05) and (d) 20% volume fraction of deionized water (denoted as 12-05-20, 14-05-20, 16-05-20, 18-05-20).

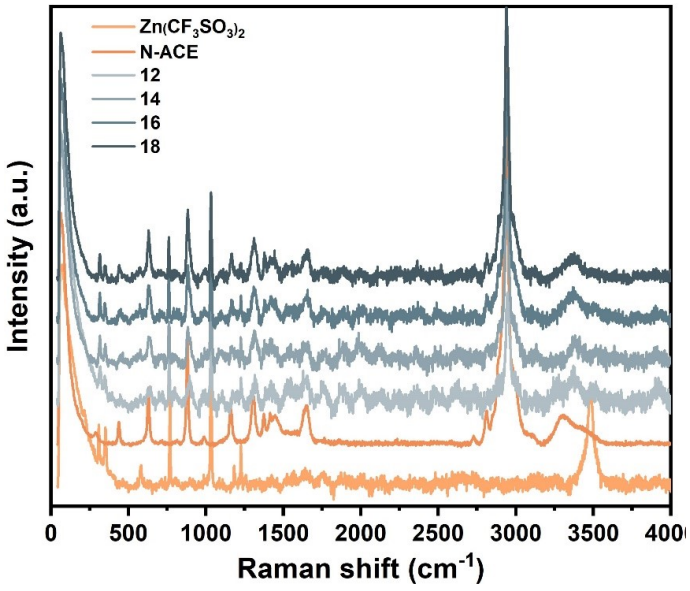

Figure S2. Raman spectra of $Zn(CF_3SO_3)_2$/N-ACE eutectic solutions with different molar ratios.

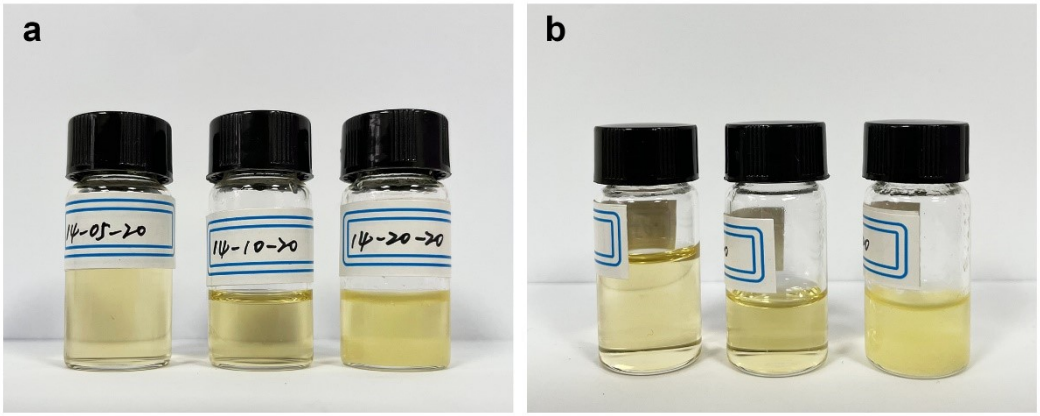

Figure S3. Optical images of mixtures based on $Zn(CF_3SO_3)_2$/N-ACE with molar ratios of 1:4 and 20% volume fraction of deionized water (14-20) after adding different concentrations (0.5M, 1.0M, 2.0M) of KI (denoted as 14-05-20, 14-10-20, 14-20-20).

It can be observed that the turbidity appeared in14-20 eutectic solution with 2.0M KI, indicating the limited solubility of KI in this system. Therefore, the concentration of KI in the eutectic solution was set as 0.5M to ensure the reversibility of the iodine redox reaction.

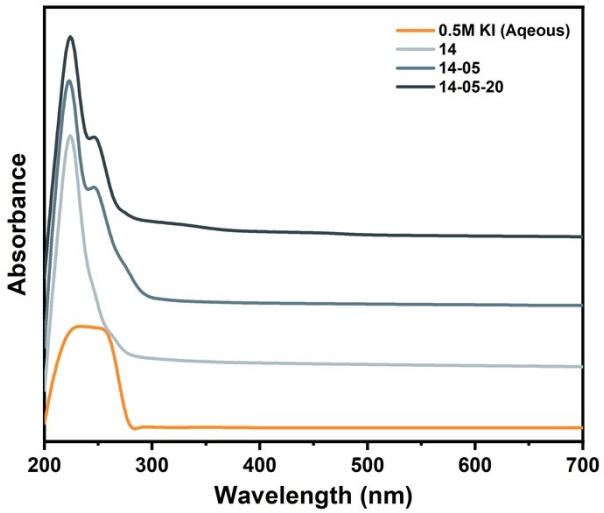

Figure S4. UV-Vis adsorption spectra of 0.5M KI in deionized water and eutectic solvents.

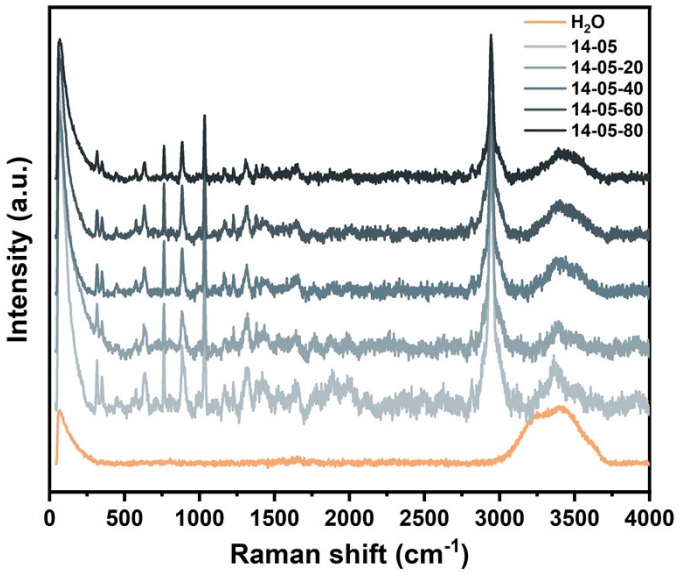

Figure S5. Raman spectra of 14-05 solutions added with different volume fractions of deionized water.

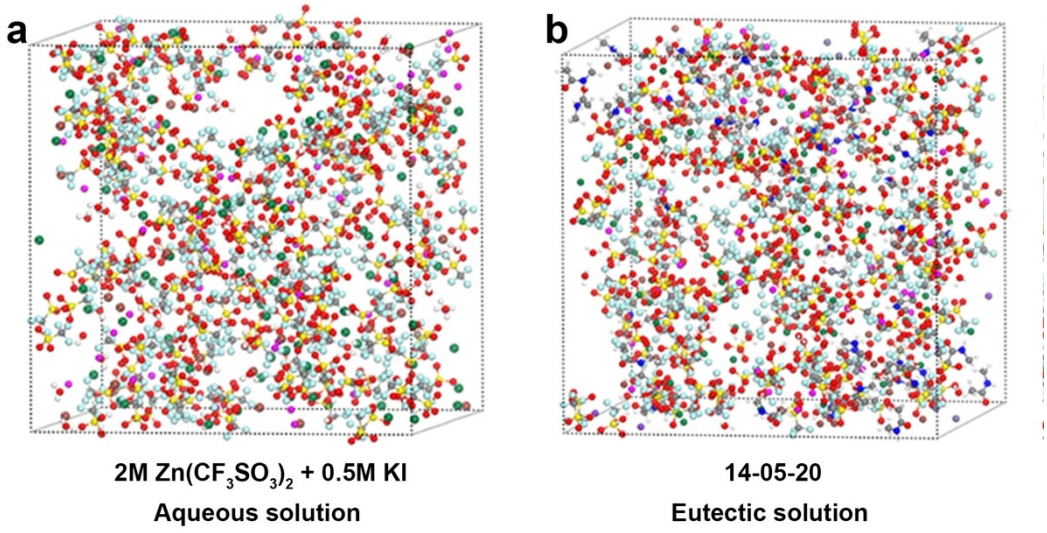

Figure S6. 3D snapshot obtained by MD simulations of (a) 2M $Zn(CF_3SO_3)_2$ + 0.5M KI aqueous and (b) 14-05-20 eutectic solutions.

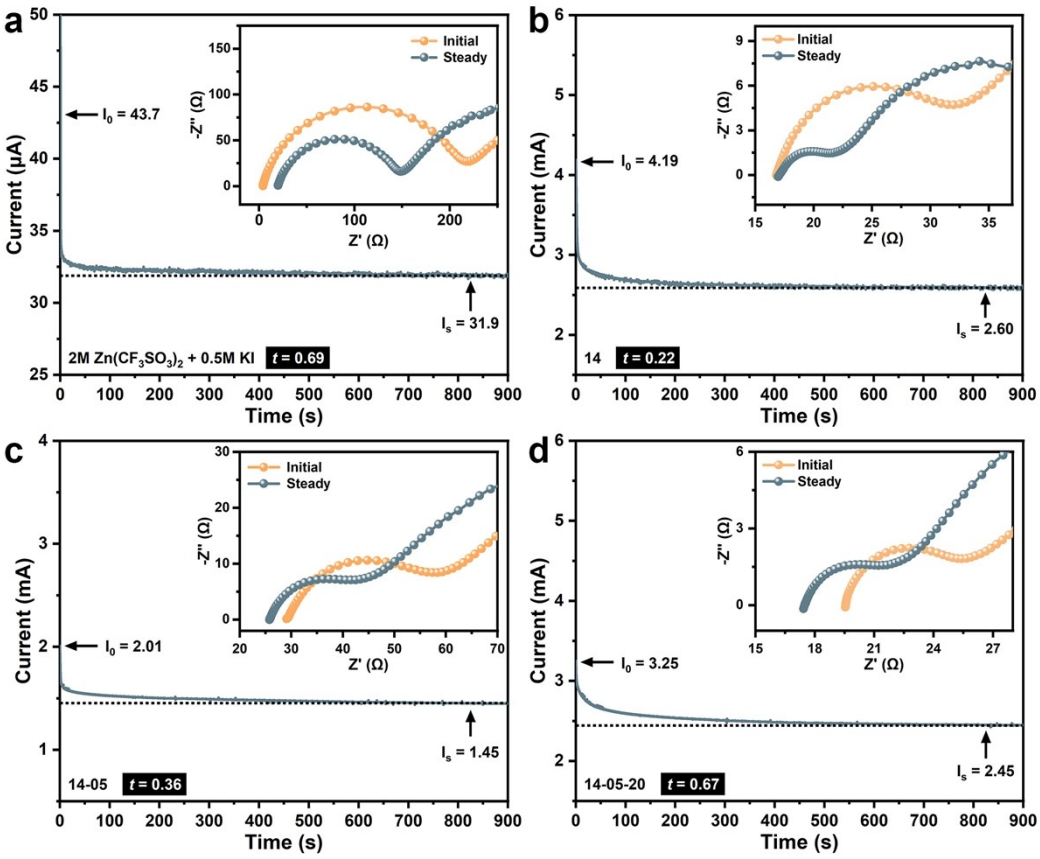

Figure S7. Chronoamperometry (CA) curves with a polarization voltage of 100 mV in zinc symmetric cells used (a) aqueous solution (2M $Zn(CF_3SO_3)_2$ + 0.5M KI) and (b-d) eutectic solutions (14, 14-05, 14-05-20) as electrolytes, respectively. The insets are the corresponding electrochemical impedance spectroscopy (EIS) spectra before and after the polarization.

The transference number of Zn^{2+} ($t_{Zn^{2+}}$) was calculated based on the chronoamperometry (CA) at polarization voltage of 100 mV and the electrochemical impedance spectroscopy (EIS) before and after the polarization of zinc symmetric cells.[1, 2] The formula is as follows:

$$t_{Zn^{2+}} = \frac{I^s R_b^s \left(\Delta V - I^0 R_i^0\right)}{I^0 R_b^0 \left(\Delta V - I^s R_i^s\right)}$$

in which ΔV represents the polarization voltage (V), and I^0, I^s correspond to the currents (A) in initial and steady state in the CA measurement. The R_b^0, R_b^s and R_i^0, R_i^s correspond to the bulk resistances (Ω) and interfacial resistances (Ω) between the electrolyte and electrode in initial and steady state, respectively, which were performed by EIS measurement.

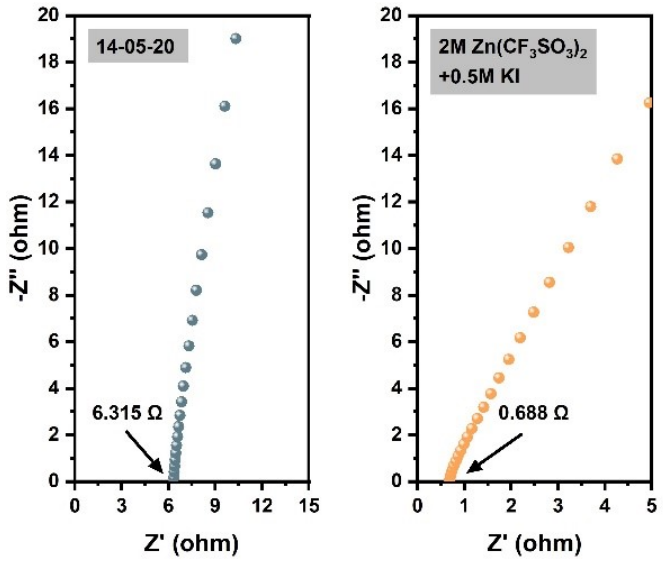

Figure S8. The EIS spectra of battery with eutectic and aqueous solutions, respectively.

The ionic conductivity of aqueous (2M $Zn(CF_3SO_3)_2$ + 0.5M KI) and eutectic (14-05-20) solutions were carried out using coin cell (CR2025) with stainless steel as electrodes, which was calculated as follow:

$$\sigma = \frac{l}{RA}$$

in which l, R and A represent the thickness, the bulk resistance and the covered area of electrolyte, respectively. The bulk resistance among them was measured on the MULTI AUTOLAB M204 in the frequency ranging from 100 kHz to 0.01 kHz. Combined the thickness of 0.043 cm and the covered area of 1.96 cm^{-2}, the ionic conductivities of aqueous and eutectic solutions are calculated to be 3.19 $\times 10^{-2}$ and 3.47 $\times 10^{-3}$ S cm^{-1}, respectively.

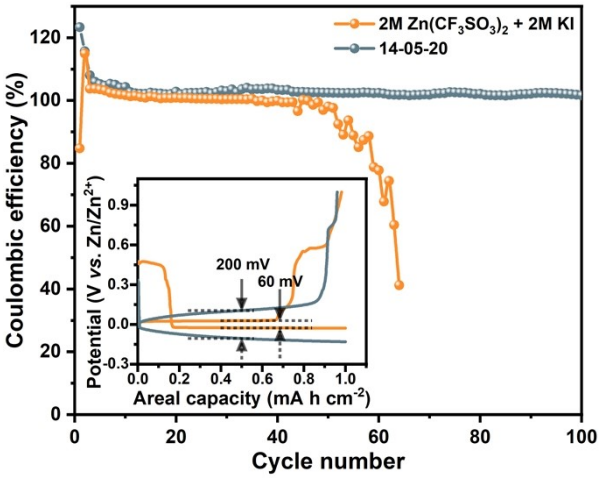

Figure S9. Coulombic efficiencies of Zn plating/stripping in aqueous and eutectic electrolytes at 1 mA cm^{-2} with a capacity limitation of 1 mA h cm^{-2}, respectively. The inset are the corresponding voltage curves in the 5th cycles.

The efficiency of Zn plating/stripping was measured by galvanostatic cycles with Zn-Cu half cells. In each cycle, 1 mA h cm^{-2} of Zn was plated on the Cu electrode at the current density of 1 mA cm^{-2}, and then stripped at the same current density until the potential reached 1 V vs. Zn^{2+}/Zn.

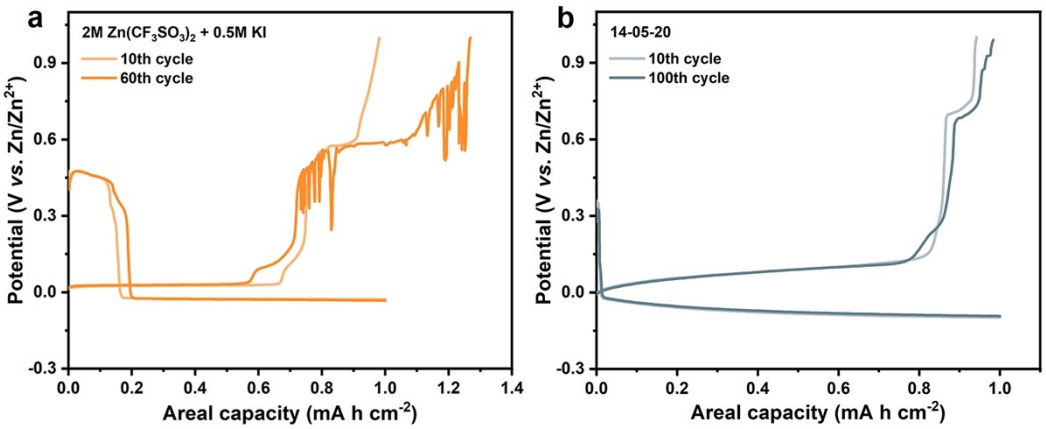

Figure S10. Galvanostatic voltage curves of Zn-Cu half cells with aqueous (10th and 60th cycles) and eutectic (10th and 100th cycles) electrolytes at 1 mA cm^{-2}, respectively.

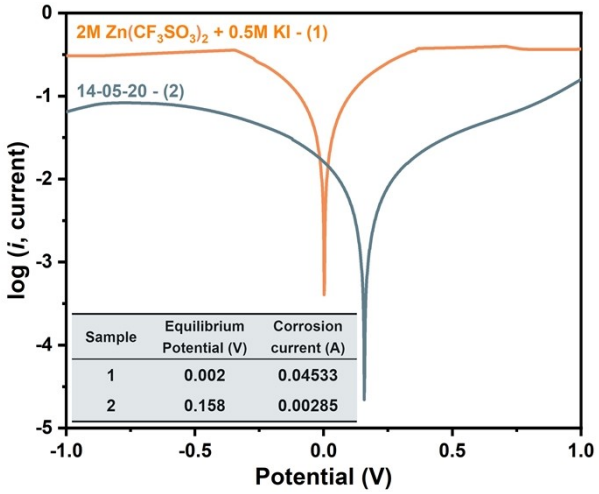

Figure S11. Tafel curves at 10 mV s^{-1} in zinc symmetric cells with aqueous and eutectic electrolytes.

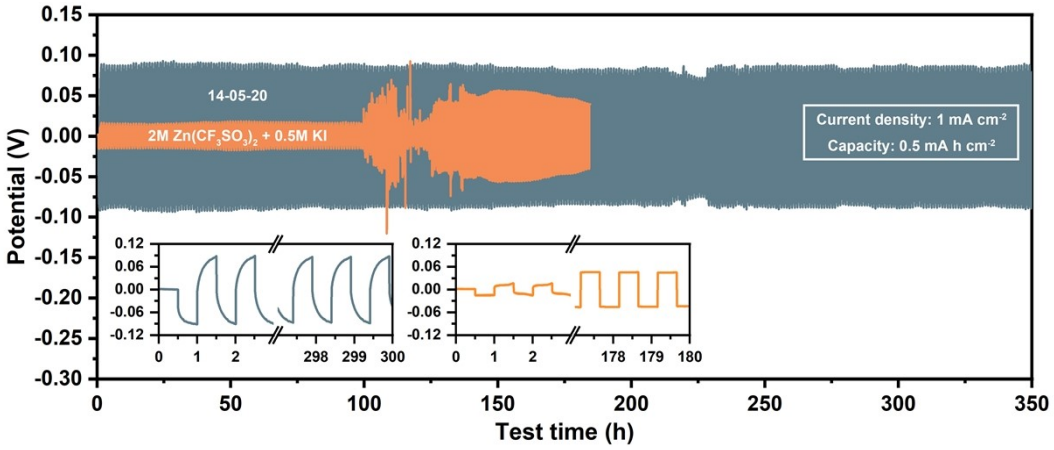

Figure S12. Galvanostatic cycling performance at the current density of 1 mA cm^{-2} to 0.5 mA h cm^{-2} in zinc symmetric cells with 14-05-20 and aqueous electrolytes.

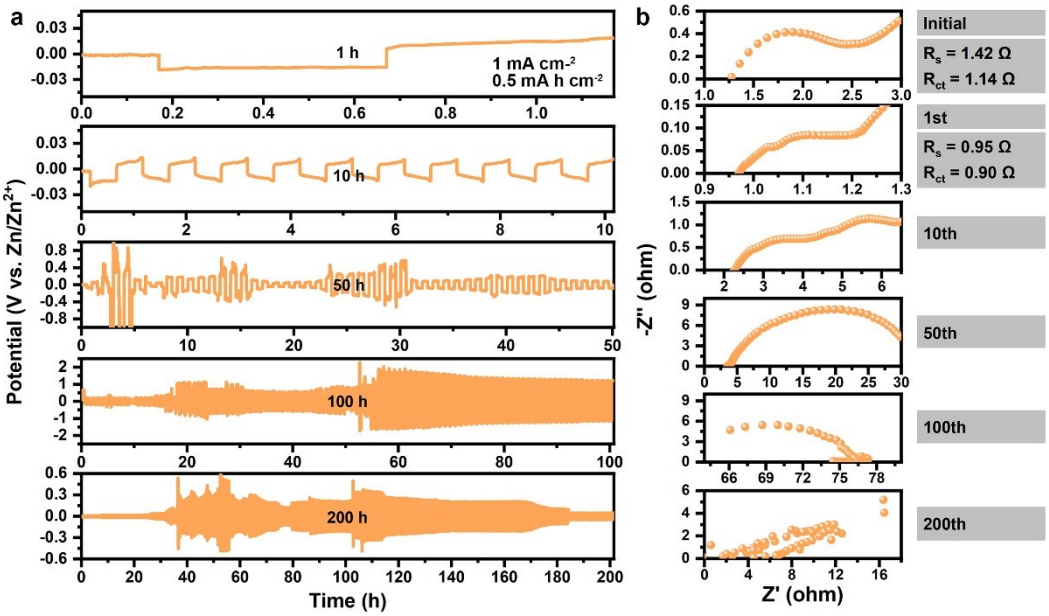

Figure S13. (a) Galvanostatic cycling performances at the current density of 1 mA cm^{-2} to 0.5 mA h cm^{-2} and (b) corresponding EIS spectra in different cycles in zinc symmetric cells with 2M $Zn(CF_3SO3)_2$ + 0.5M KI electrolyte, respectively.

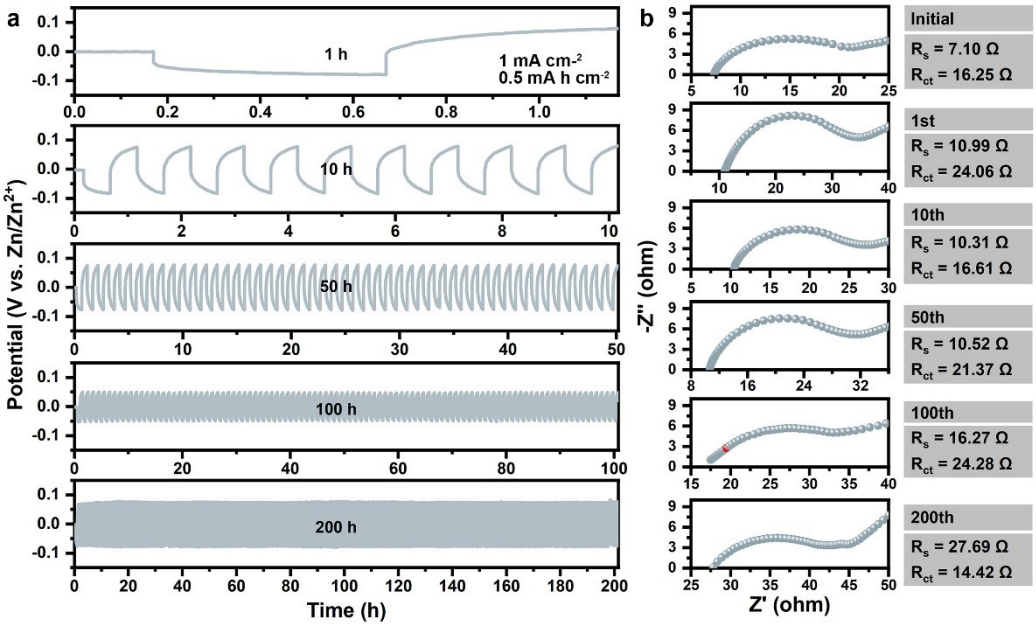

Figure S14. (a) Galvanostatic cycling performances at the current density of 1 mA cm^{-2} to 0.5 mA h cm^{-2} and (b) corresponding EIS spectra in different cycles in zinc symmetric cells with 14-05-20 electrolyte, respectively.

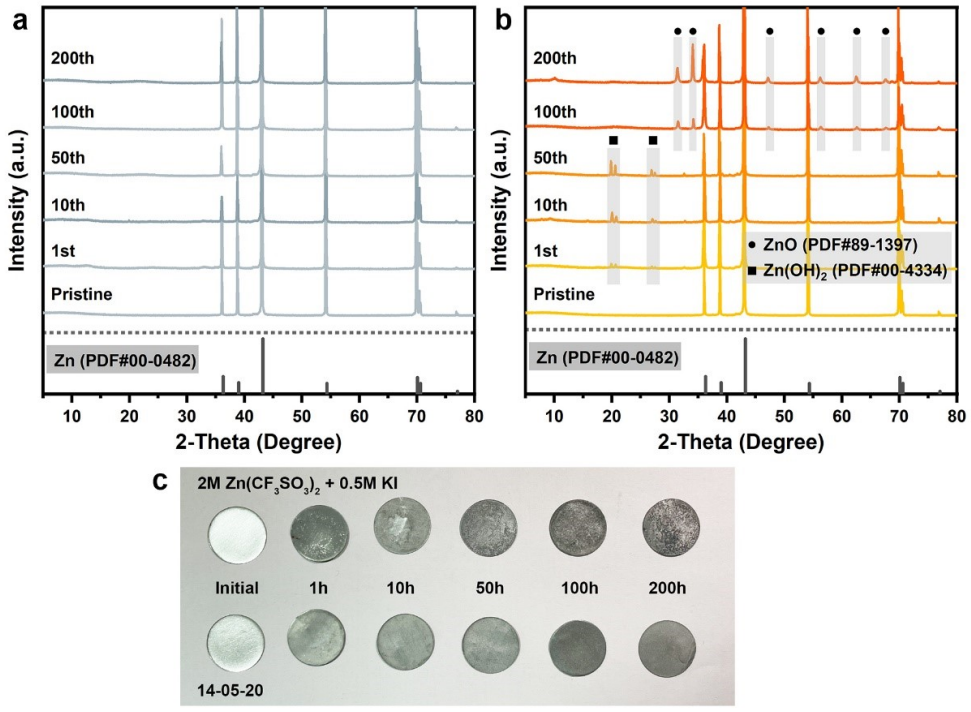

Figure S15. (a, b) XRD patterns and (c) optical images of anode in different cycles of zinc symmetric cells used aqueous and 14-05-20 electrolytes, respectively.

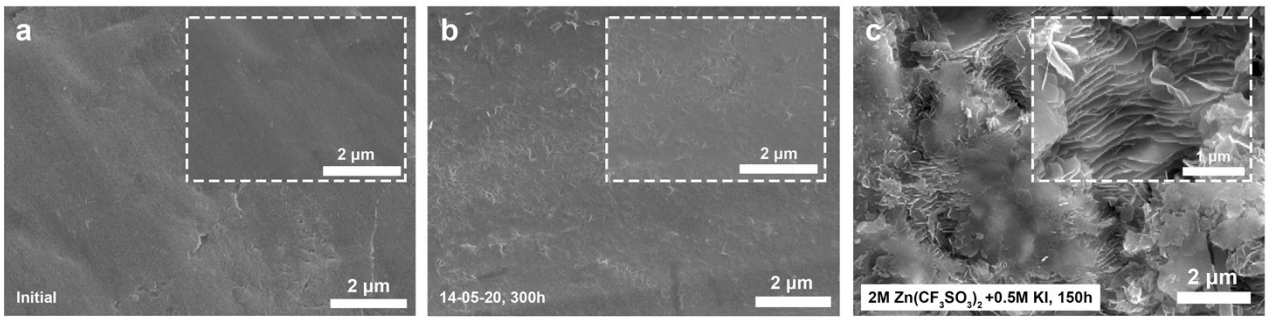

Figure S16. SEM images of anodic zinc in (a) initial and zinc symmetric cells under the galvanostatic conditions for 300 h with (b) 14-05-20, (c) aqueous electrolytes, respectively.

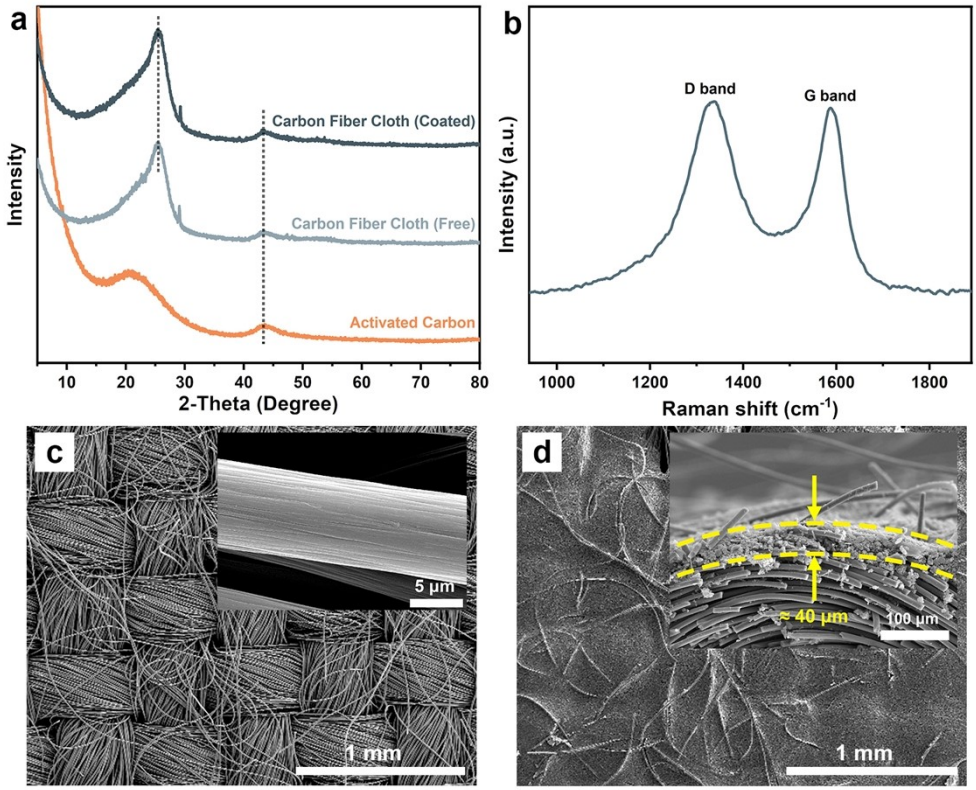

Figure S17. XRD patterns, Raman spectra and SEM images of activated carbon-coated carbon fiber cloth (AC/CFC) cathode.

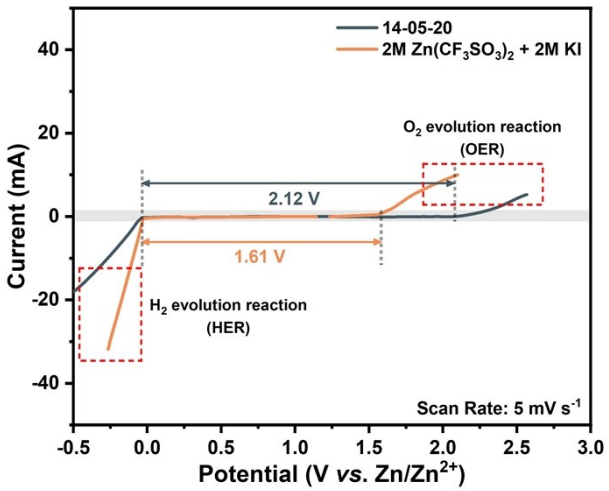

Figure S18. Linear sweep voltammetry (LSV) curves at a scan rate of 5 mV s^{-1} of Zn-CFC batteries with 14-05-20 and 2M $Zn(CF_3SO_3)_2$ + 0.5M KI electrolytes, respectively.

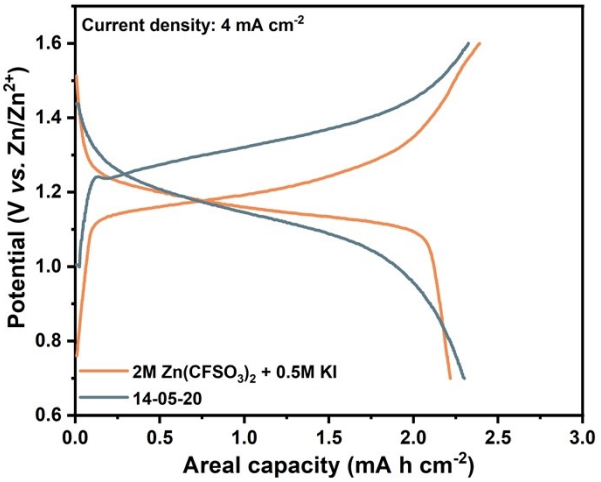

Figure S19. Galvanostatic charge/discharge curves of Zn-AC/CFC battery with different electrolytes.

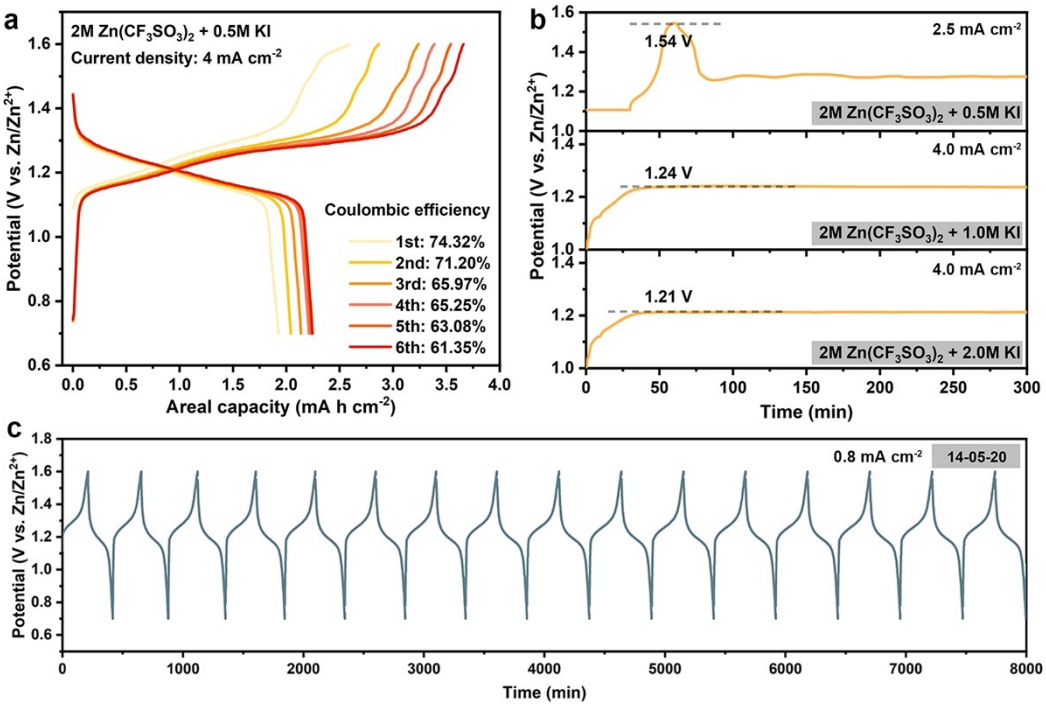

Figure S20. Galvanostatic charge/discharge curves of Zn-AC/CFC battery with (a, b) different concentration of KI (0.5M, 1.0M, 2.0M) in aqueous electrolytes (2M $Zn(CF_3SO_3)_2$) and (c) 14-05-20 electrolyte, respectively.

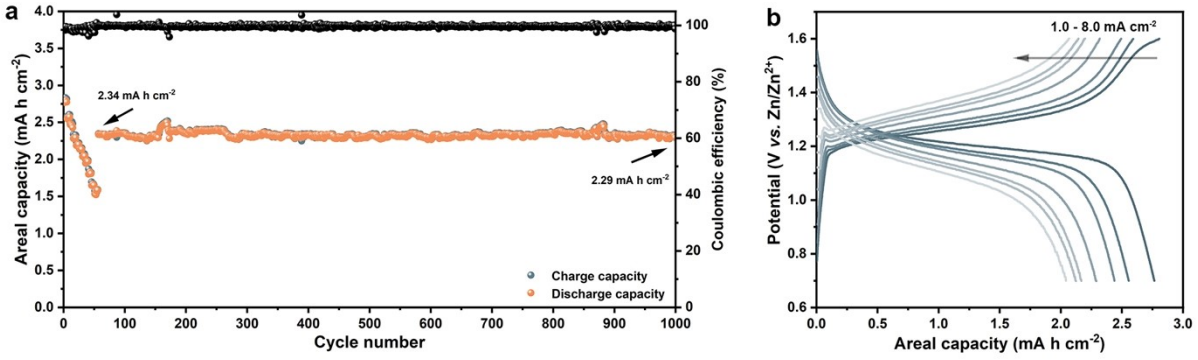

Figure S21. (a) Rate performance from 1.0 to 16.0 mA cm^{-2} and (b) corresponding galvanostatic curves of Zn-AC/CFC battery with 14-05-20 electrolyte.

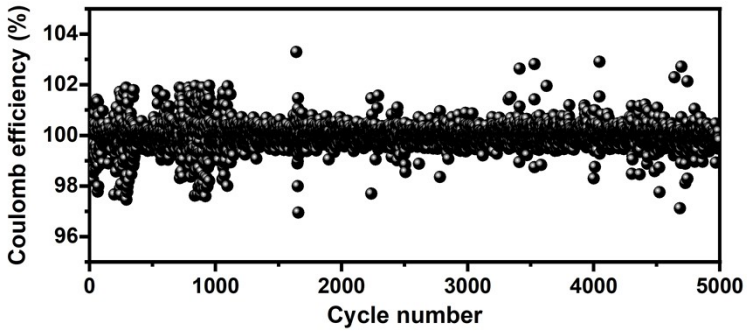

Figure S22. The details in coulombic efficiency of Zn-AC/CFC battery with 14-05-20 electrolyte during the long-term cycling performance at 4 mA cm^{-2}.

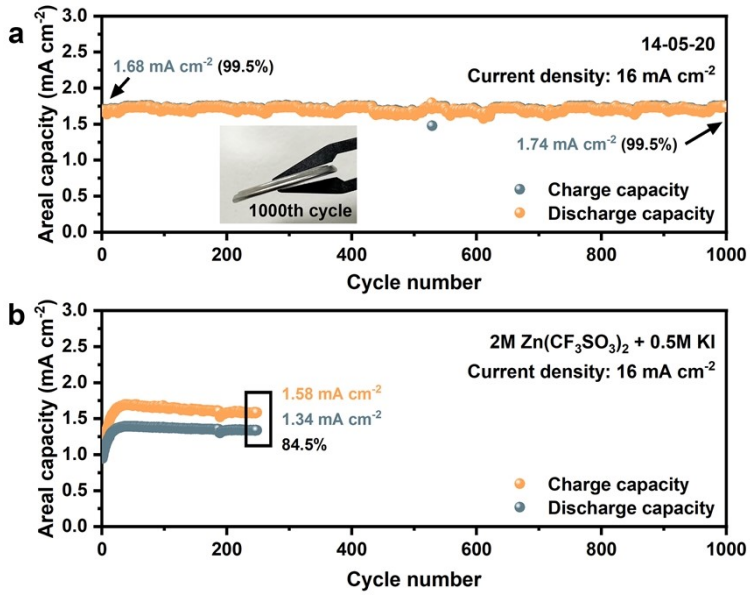

Figure S23. Cycling performance at 16 mA cm^{-2} and corresponding optical image in the 1000th cycle of Zn-AC/CFC batteries with 14-05-20 and aqueous electrolytes, respectively.

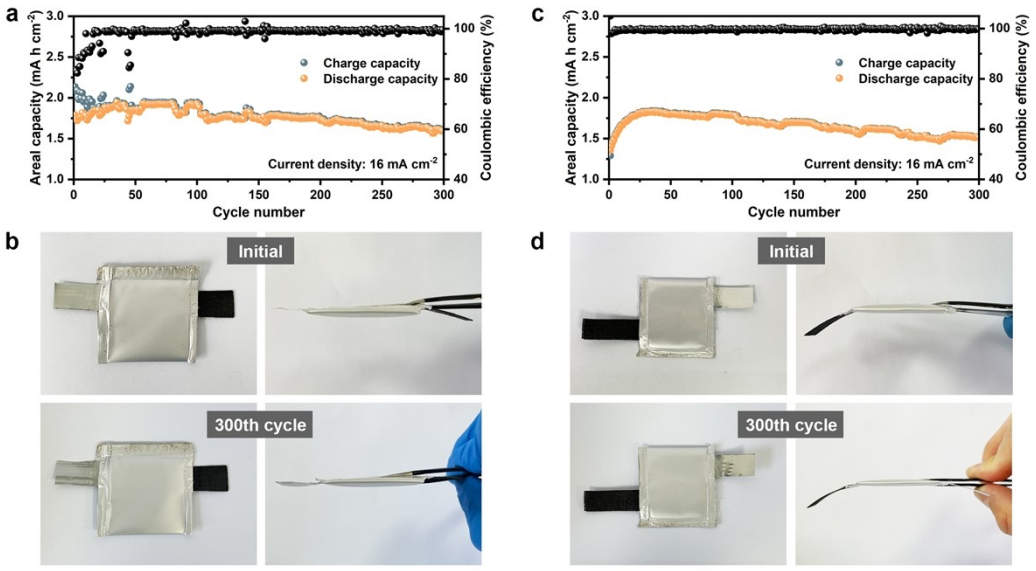

Figure S24. Cycling performance at 16 mA cm^{-2} and corresponding optical images before and after the measurement of soft package battery with 14-05-20 electrolyte (a, b: sample 1; c, d: sample 2).

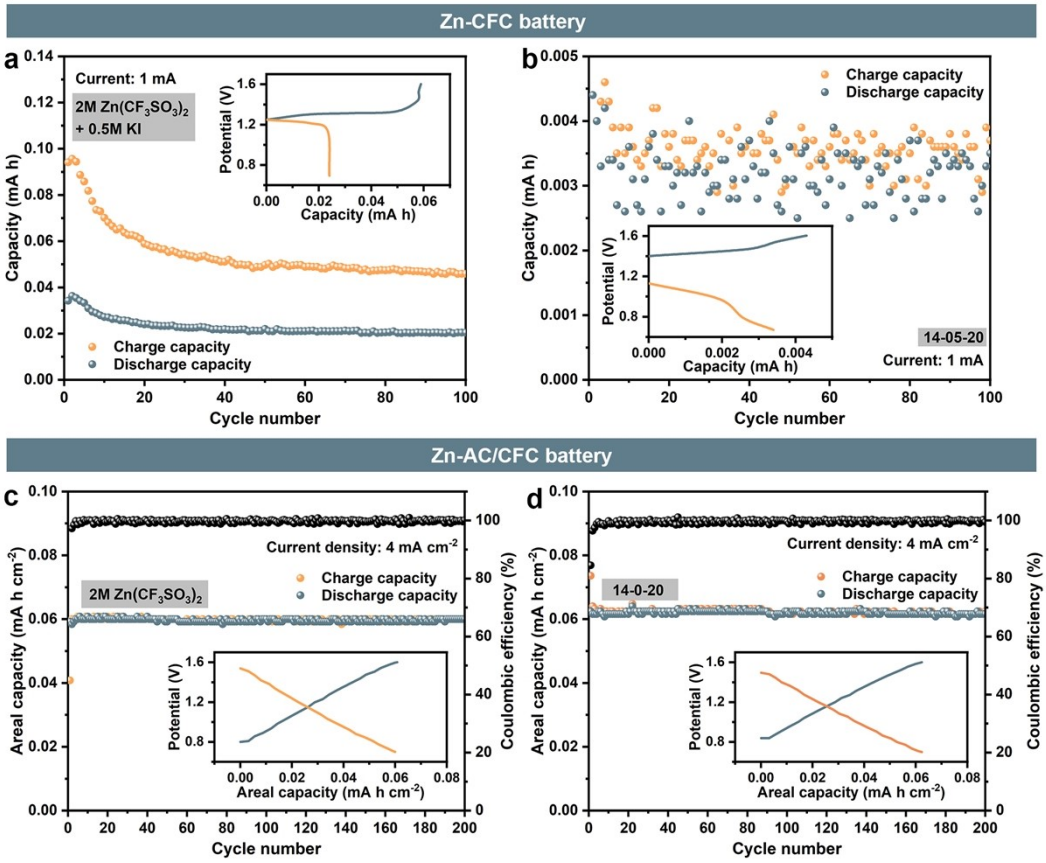

Figure S25. The electrochemical performances and galvanostatic charge/discharge curves of (a) Zn-CFC battery with 2M $Zn(CF_3SO_3)_2$ + 0.5M KI and 14-05-20 electrolytes and (b) Zn-AC/CFC battery with 2M $Zn(CF_3SO_3)_2$ and 14-0-20 electrolytes, respectively.

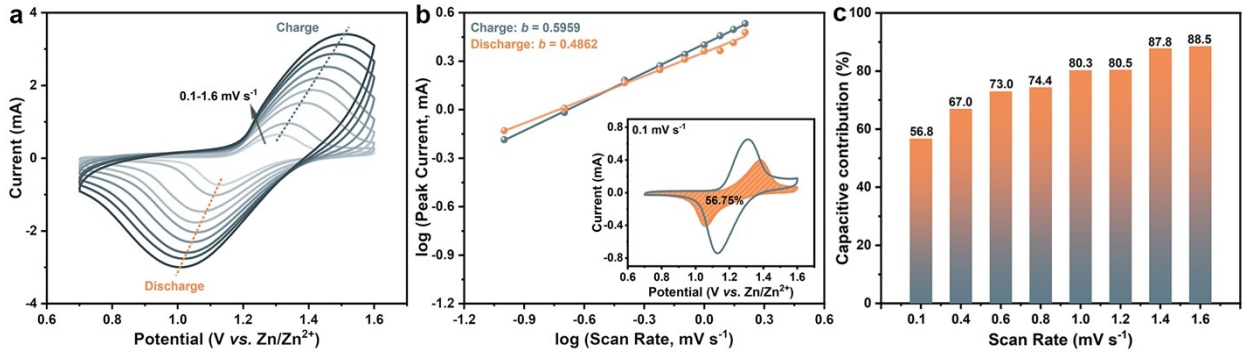

Figure S26. (a) CV curves at scan rates from 0.1 to 1.6 mV s^{-1}, (b) the corresponding *log(current) vs. log(scan rate)* plots of redox peaks with marked region of capacitive-controlled contribution at 0.1 mV s^{-1} and (c) the calculated capacitive-controlled contributions at different scan rates.

According to the research of Dunn[3], the measure current (i) and scan rate (v) in CV curves have relationships with equation:

$$i = av^b$$

$$log(i) = b \times log(v) + log(a)$$

Where a, b are adjustable parameters in which the value of b is between 0.5 and 1, in which the b value of 0.5 indicates a full diffusion-controlled process and $b = 1$ corresponds to the full capacitive contribution. Also, the values of b can be obtained by calculating the slope of the *log(i) vs. log(v)* plots.

Meanwhile, the contribution of pseudocapacitive can be quantified by the equations:[3-5]

$$i = k_1 v + k_2 v^{1/2}$$

$$i/v^{1/2} = k_1 v^{1/2} + k_2$$

Where the capacity contribution can be divided into capacitive (measured with k_1) and diffusion-controlled (measured with k_2). By determining values of both k_1 and k_2, we can distinguish the fraction of the current from surface capacitance and diffusion limitted.[6]

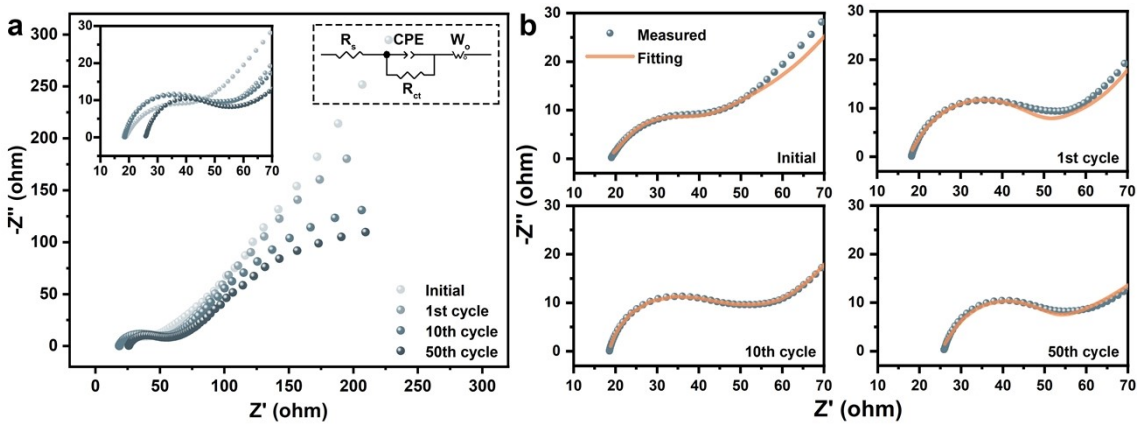

Figure S27. The EIS spectra at different cycles of Zn-AC/CFC battery with 15-05-20 electrolyte.

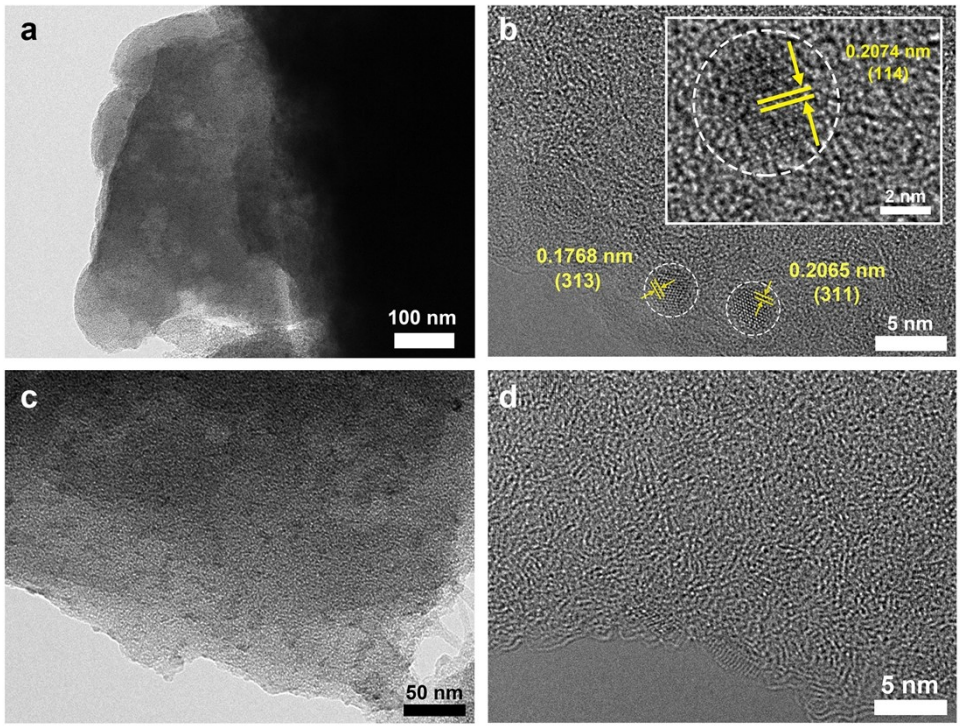

Figure S28. The transmission electron microscope (TEM) and high-resolution transmission electron microscopy (HRTEM) images of AC/CFC cathode at (a, b) fully charged and (c, d) discharged states with 14-05-20 electrolyte.

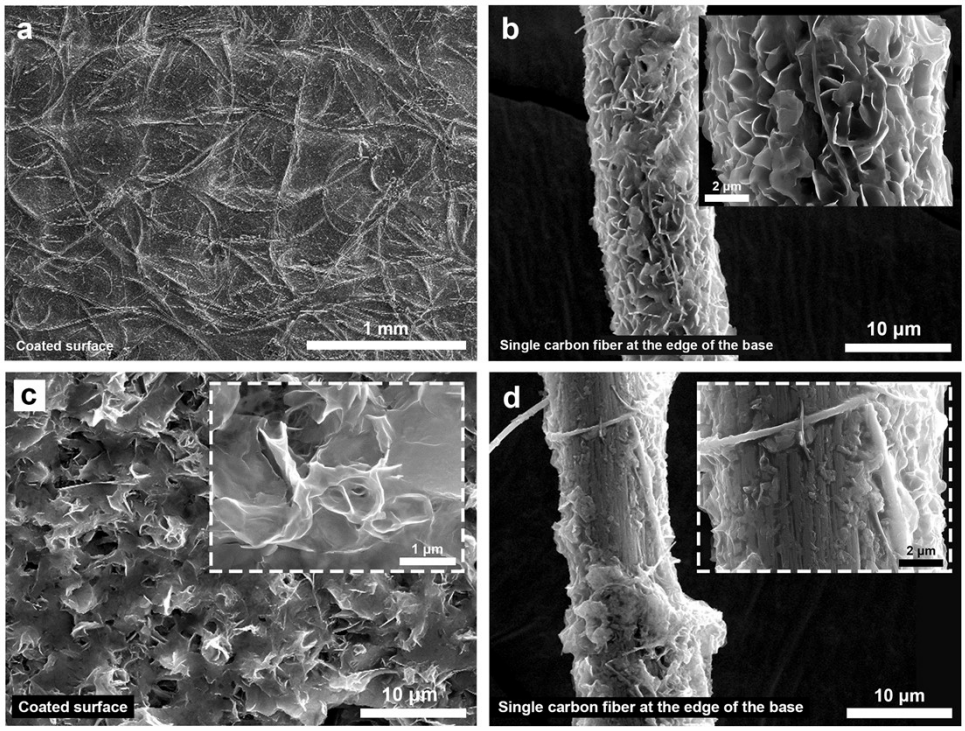

Figure S29. SEM images of uncleaned cathodes after 50 cycles in the Zn-AC/CFC battery with (a, b) 14-05-20 and (c, d) aqueous electrolytes, respectively.

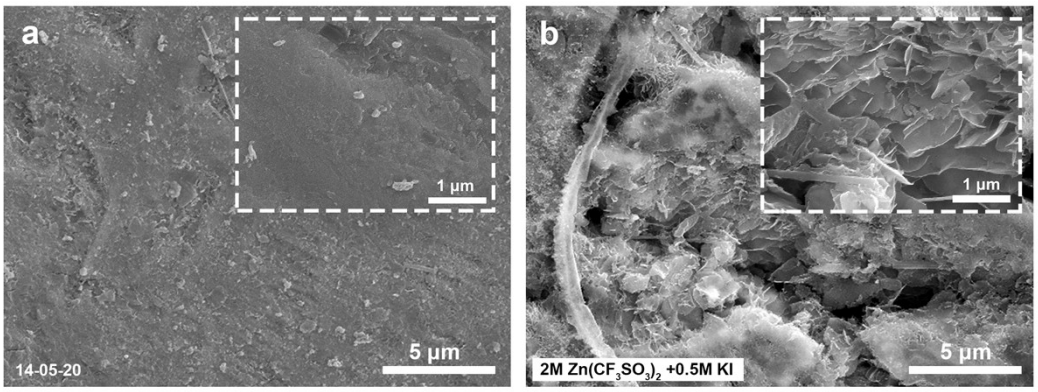

Figure S30. SEM images of anode after 50 cycles in Zn-AC/CFC battery with (a) 14-05-20 and (b) aqueous electrolytes, respectively.

Table S1. The fitting ohmic resistances (R_s) and charge transfer resistances (R_{ct}) from the EIS results of Zn-AC/CFC with 14-05-20 electrolyte.

Cycle	R_s (Ω)	R_{ct} (Ω)
Initial	17.59	11.45
1st	17.14	26.10
10th	17.63	36.46
50th	24.43	20.30

Reference

1. J. Evans, C. A. Vincent and P. G. Bruce, *Polymer*, 1987, **28**, 2324-2328.
2. K. M. Abraham, Z. Jiang and B. Carroll, *Chem. Mater.*, 1997, **9**, 1978-1988.
3. J. Wang, J. Polleux, J. Lim and B. Dunn, *J. Phys. Chem. C*, 2007, **111**, 14925-14931.
4. T. Brezesinski, J. Wang, S. H. Tolbert and B. Dunn, *Nat. Mater.*, 2010, **9**, 146-151.
5. D. Chao, C. Zhu, P. Yang, X. Xia, J. Liu, J. Wang, X. Fan, S. V. Savilov, J. Lin, H. J. Fan and Z. X. Shen, *Nat. Commun.*, 2016, **7**, 12122.
6. P. He, M. Yan, G. Zhang, R. Sun, L. Chen, Q. An and L. Mai, *Adv. Energy Mater.*, 2017, **7**, 1601920.